

RESEARCH ARTICLE

Dync1li1 is required for the survival of mammalian cochlear hair cells by regulating the transportation of autophagosomes

Yuan Zhang^{1,2}✉, Shasha Zhang³✉*, Han Zhou¹, Xiangyu Ma³, Leilei Wu³, Mengyao Tian³, Siyu Li¹, Xiaoyun Qian^{1,2}*, Xia Gao^{1,2}*, Renjie Chai^{3,4,5,6,7}*

1 Department of Otolaryngology Head and Neck Surgery, Affiliated Drum Tower Hospital of Nanjing University Medical School, Jiangsu Provincial Key Medical Discipline (Laboratory), Nanjing, China, **2** Research Institute of Otolaryngology, Nanjing, China, **3** State Key Laboratory of Bioelectronics, Department of Otolaryngology Head and Neck Surgery, Zhongda Hospital, School of Life Sciences and Technology, Advanced Institute for Life and Health, Jiangsu Province High-Tech Key Laboratory for Bio-Medical Research, Southeast University, Nanjing, China, **4** Department of Otolaryngology Head and Neck Surgery, Sichuan Provincial People's Hospital, University of Electronic Science and Technology of China, Chengdu, China, **5** Co-Innovation Center of Neuroregeneration, Nantong University, Nantong, China, **6** Institute for Stem Cell and Regeneration, Chinese Academy of Science, Beijing, China, **7** Beijing Key Laboratory of Neural Regeneration and Repair, Capital Medical University, Beijing, China

✉ These authors contributed equally to this work.

* zhangss5576@163.com (SZ); qxy522@163.com (XQ); xiagaogao@hotmail.com (XG); renjiec@seu.edu.cn (RC)



OPEN ACCESS

Citation: Zhang Y, Zhang S, Zhou H, Ma X, Wu L, Tian M, et al. (2022) Dync1li1 is required for the survival of mammalian cochlear hair cells by regulating the transportation of autophagosomes. *PLoS Genet* 18(6): e1010232. <https://doi.org/10.1371/journal.pgen.1010232>

Editor: Tal Teitz, Creighton University School of Medicine, UNITED STATES

Received: August 31, 2021

Accepted: May 3, 2022

Published: June 21, 2022

Copyright: © 2022 Zhang et al. This is an open access article distributed under the terms of the [Creative Commons Attribution License](https://creativecommons.org/licenses/by/4.0/), which permits unrestricted use, distribution, and reproduction in any medium, provided the original author and source are credited.

Data Availability Statement: All relevant data are within the manuscript and its [Supporting Information](#) files.

Funding: This work was supported by grants from National Key R&D Program of China (No. 2021YFA1101300, 2020YFA0112503) to RC. This work was funded by the National Natural Science Foundation of China (No.81970885) to XQ. This work was supported by grants from Strategic Priority Research Program of the Chinese Academy of Science (XDA16010303), National

Abstract

Dync1li1, a subunit of cytoplasmic dynein 1, is reported to play important roles in intracellular retrograde transport in many tissues. However, the roles of Dync1li1 in the mammalian cochlea remain uninvestigated. Here we first studied the expression pattern of Dync1li1 in the mouse cochlea and found that Dync1li1 is highly expressed in hair cells (HCs) in both neonatal and adult mice cochlea. Next, we used *Dync1li1* knockout (KO) mice to investigate its effects on hearing and found that deletion of Dync1li1 leads to early onset of progressive HC loss via apoptosis and to subsequent hearing loss. Further studies revealed that loss of Dync1li1 destabilizes dynein and alters the normal function of dynein. In addition, *Dync1li1* KO results in a thinner Golgi apparatus and the accumulation of LC3+ autophagic vacuoles, which triggers HC apoptosis. We also knocked down *Dync1li1* in the OC1 cells and found that the number of autophagosomes were significantly increased while the number of autolysosomes were decreased, which suggested that *Dync1li1* knockdown leads to impaired transportation of autophagosomes to lysosomes and therefore the accumulation of autophagosomes results in HC apoptosis. Our findings demonstrate that Dync1li1 plays important roles in HC survival through the regulation of autophagosome transportation.

Author summary

Hearing loss is one of the most common sensorial disorders globally. The main reason of hearing loss is the irreversible loss or malfunction of cochlear hair cells. Identifying new

Natural Science Foundation of China (Nos. 82030029, 81970882, 92149304), Natural Science Foundation from Jiangsu Province (No. BE2019711), Science and Technology Department of Sichuan Province (No. 2021YFS0371), Shenzhen Fundamental Research Program (JCYJ20190814093401920, JCYJ20210324125608022), and Open Research Fund of State Key Laboratory of Genetic Engineering, Fudan University (No. SKLGE-2104) to RC. The work was supported by grants from the National Natural Science Foundation of China (Nos. 81970892, 82171149), the Natural Science Foundation of Jiangsu Province (Nos. BK20190062), and the Fundamental Research Funds for the Central Universities for the Support Program of Zhishan Youth Scholars of Southeast University (Nos. 2242021R41136) to SZ. The work was funded by the Major Program of National Natural Science Foundation of China (82192862) to XG. The funders had no role in study design, data collection and analysis, decision to publish, or preparation of the manuscript.

Competing interests: The authors have declared that no competing interests exist.

hearing loss-related genes and investigating their roles and mechanisms in HC survival are important for the prevention and treatment of hereditary hearing loss. Cytoplasmic dynein 1 is reported to play important roles in ciliogenesis and protein transport in the mouse photoreceptors. Here, we described the expression pattern of Dyncili1 (a subunit of cytoplasmic dynein 1) in the mouse cochlea and used knockout mice to investigate its specific role in the hair cell of cochlea.

Introduction

Hearing loss is one of the most common sensorial disorders globally, and it leads to reduced quality of daily life and to huge economic costs [1]. Genetic factors, aging, intense noise exposure, and aminoglycoside treatment can cause hearing loss, mainly through the irreversible loss or malfunction of cochlear hair cells (HCs) [2]. Genetic factors causing hereditary hearing loss remain to be identified. Therefore, identifying new hearing loss-related genes and investigating their roles and mechanisms in HC survival are important for the prevention and treatment of hereditary hearing loss.

Cytoplasmic Dynein1 (hereafter referred to as dynein), responsible for intracellular retrograde transport, is a multi-subunit complex that consists of two copies of the 530 kDa dynein heavy chain (DHC), two 74 kDa dynein intermediate chains (DICs), two 53–57 kDa dynein light intermediate chains (DLICs), and three 8–21 kDa light chains (DLCs) [3,4]. The DHC harbors the ATPase and is responsible for force production. The DIC plays a key scaffolding role in the complex and is involved in communicating with other protein complexes to regulate dynein activity [3,5]. It is reported that the DLC can act as an adapter to link various proteins to the dynein motor complex [6–8]. The DLIC is an essential subunit of dynein and is highly conserved in different eukaryotic cells [9]. In vertebrates, there are two DLIC genes, *Dync1li1* and *Dync1li2*, while there is only one DLIC gene in lower eukaryotes [10,11]. The C-terminus of the DLIC contains two conserved regions with helical propensity, and the N-terminal GTPase-like domain is also conserved and tightly binds to the DHC [7,12,13]. Knock-down (KD) or knockout (KO) of *Dync1li1* in vitro leads to mitotic defects, fragmentation of the Golgi apparatus, and abnormal intracellular vesicle transport [14–17], and depletion of *Dync1li1* in *Drosophila* cells and *Aspergillus nidulans* leads to destabilization of the DHC and DIC [14,18]. Mice with a point mutation in *Dync1li1* show increased length of dendrites in cortical neurons and an increased number of dendrite branches in dorsal root ganglia neurons [19]. In the retina, *Dync1li1* regulates the transportation of membrane proteins of rod outer segment from the Golgi to the base of the connecting cilium, thus regulating the formation of primary cilia [20]. Considering that the retina and the cochlea are both sensorial organs and might share some common mechanisms, we hypothesize that *Dync1li1* plays important roles in the cochlea.

Autophagy is a highly conserved homeostatic process that eliminates defective organelles and misfolded proteins [21–23]. Several studies have suggested that there is a close relationship between autophagy and hearing loss in animal models [24–26]. Autophagic flux includes autophagosome formation, transportation and fusion with the lysosome, and finally maturation to form autolysosomes (both autophagosome and autolysosomes are called autophagic vacuoles) [27]. Disruption of autophagic flux will prevent autophagosomes from being cleared from the cell, thus resulting in increased cellular stress and ultimately leading to cell death and subsequent neurodegenerative disorders [28–30]. Current research on autophagy in the

auditory system is limited, and most such studies have focused on sensorineural hearing loss caused by exogenous HC damage [31].

It has been widely reported that there is a close relationship between dynein and autophagy [32]. When autophagy is induced due to nutrient starvation *in vitro*, DLCs help to release autophagic regulators from the dynein complex and thus initiate autophagosome nucleation [33,34]. In the brain, the impairment of dynein-driven autophagosome motility causes autophagosomes to accumulate in neurites and synaptic termini, and this indicates the importance of dynein and autophagy in the clearance of aggregate-prone proteins in preventing neurodegenerative diseases [35–39]. However, the relationships between dynein and autophagy in the inner ear remain to be investigated.

To understand the role of Dync1li1 in cochlear HCs and to elucidate the relationship between dynein and autophagy in the inner ear, we determined the expression pattern of Dync1li1 in the inner ear and investigated its role and mechanism in hearing function by using *Dync1li1* KO mice [20]. We found that Dync1li1 is highly expressed in HCs in both neonatal and adult mice and that *Dync1li1* KO leads to progressive HC loss via apoptosis and subsequently leads to hearing loss. We also found that deletion of *Dync1li1* resulted in a reduced number of Golgi lamellae and the accumulation of autophagosomes both *in vitro* and *in vivo*, which suggested that deletion of *Dync1li1* leads to HC apoptosis due to impaired transportation of autophagosomes. Overall, we provide evidence that Dync1li1 plays important roles in HC survival by regulating autophagosome transportation and Golgi-related vesicle trafficking.

Materials and methods

Ethics statement

Animals were maintained following the Rutgers University Institutional Animal Use and Care Committee (Protocol 201702497), National Institutes of Health guidelines, and the policies of the Expert Committee for the Approval of Projects of Experiments on Animals of the Academy of Sciences of the Czech Republic (Protocol 43/2015). These regulatory bodies approved all experimental procedures involving the animals.

All animal procedures were performed according to the protocols that were approved by the Animal Experimental Ethical Inspection Form of Southeast University (No.20210302028). All animal procedures were consistent with the National Institute of Health's Guide for the Care and Use of Laboratory Animals.

Animals

Dync1li1 KO mice were a gift from Prof. Wufan Tao (Fudan University, Shanghai, China) [20]. LC3-GFP reporter mice of both sexes in the C57BL/6JNju background (Stock D000244, Nanjing Biomedical Research Institute of Nanjing University) were used in the experiments.

Genotyping PCR

LC3-GFP reporter mice were genotyped by using genomic DNA from tail tips. Tail tips were digested by adding 180 μ l 50 mM NaOH, incubating at 98°C for 1 h, and adding 20 μ l 1M Tris-HCl pH 7.0. The genotyping primers were used as follows: wild type (F) 5'-TGA GCG AGC TCA AGA TAA TCA GGT-3'; wild type (R) 5'-GTT AGC ATT GAG CTG CAA GCG CCG TCT-3'; mutant (F): 5'-TCC TGC TGG AGT TCG TGA CCG-3'; mutant (R): 5'-TTG CGA ATT CTC AGC CGT CTT CAT CTC TCT CGC-3'. The PCR system for genotyping is as follows: genomic DNA 3 μ l, primer of each 0.5 μ l, 2 \times PCR mix (Vazyme, P112-03) 10 μ l, and add H₂O up to a total volume of 20 μ l. The conditions of PCR were an initial denaturing

step of 3 min at 94°C followed by 35 cycles of 35 s denaturation at 94°C, 30 s annealing at 60°C, and 40 s extension at 72°C. Genotyping of Dync1li1 KO mice was performed according to the previous report [20]. The genotyping primers of Dync1li1 were used as follows: wild type (F) 5'-GGA AGA TGT GAC AAG ACA GAC ACG -3'; wild type (R) 5'-TGG CTC AGT GGT AAA GGT CC -3'; mutant (F): 5'-GGA AGA TGT GAC AAG ACA GAC ACG -3'; mutant (R): 5'-TCA GGA AAA GCA CTG GCT G -3'.

Auditory brainstem response (ABR) test

The mice were injected I.P. with 0.01 g/ml pentobarbital sodium (100 mg/kg body weight) to achieve deep anesthesia, and the closed-field ABR test were measured for thresholds is previously described [40]. The ABR test was performed in a soundproof room, and 3 fine needle-like electrodes were inserted at the cranial vertex, underneath the ear, and at the back near the tail of the mice. The frequency of ABR test are 4 kHz, 8 kHz, 12 kHz, 16 kHz, 24 kHz, and 32 kHz. The hearing thresholds were determined by decreasing the sound intensities from 90 dB in 20 dB steps until the lowest sound intensity of the first wave could be identified. All test was measured by TDT System III workstation running SigGen32 software (Tucker-Davis Technologies). The data were analyzed by using GraphPad Prism 7 software.

Immunostaining and image acquisition

For P0–P7 neonatal mice, the cochlea was dissected with sharp forceps (WPI) in cold HBSS and the tissue fixed in 4% paraformaldehyde (PFA) for 1 h at room temperature (RT). When mice older than P7, the temporal bone was fixed in 4% PFA for 1 h, decalcified in 0.5 M EDTA solution for 1–3 days (it depends on the mice age) at RT, and then dissected in HBSS. The sample was washed by PBS and then blocked with blocking medium (5% donkey serum, 0.5% Triton X100, 0.02% sodium azide, and 1% bovine serum albumin in pH 7.4 PBS) for 1 h at RT. And then incubated with primary antibodies diluted in PBT1 medium (2.5% donkey serum, 0.1% Triton X100, 0.02% sodium azide, and 1% bovine serum albumin in pH 7.4 PBS) at 4°C overnight. The sample was then washed with 0.1% Triton X100 in pH 7.4 PBS for three times and incubated with fluorescence-conjugated secondary antibody (Invitrogen) or phalloidin (Invitrogen), both diluted 1:400 in PBT2 medium (0.1% Triton X100 and 1% bovine serum albumin in pH 7.4 PBS), for 1 h at RT. The sample was mounted in antifade fluorescence mounting medium (DAKO) after washing with 0.1% Triton X100 in pH 7.4 PBS for three times. The primary antibodies were anti-Myo7a (rabbit anti-my7a; Proteus Bioscience, #25–6790; 1:1000 dilution in PBT1), phalloidin (Invitrogen, A34055), DAPI (Solarbio, C0060), anti-Dync1li1 (Abcam, ab157468, 1:400 dilution in PBT1), anti-Ctbp2 (BD Biosciences, #612044, 1:400 dilution in PBT1), anti-PSD95 (Millipore, #MAB1596, 1:400 dilution in PBT1), anti-Rab7 (abcam, ab137029, 1:400 dilution in PBT1). A TUNEL kit (Roche, 11684817910) was used to detect apoptotic cells according to the instructions. For image acquisition, all samples were scanned by Zeiss microscope (LSM 710) with the same hardware settings to enable direct comparison between treatment conditions. Since synapses are not always on the same layer, we performed Z projection with ImageJ software to capture the Ctbp2 (presynaptic marker) and PSD95 (postsynaptic marker) staining images in S3 Fig. HEI-OC1 cell immunohistochemistry protocol was the same as above.

Scanning electron microscopy (SEM) and transmission electron microscopy (TEM)

As previously described [41], Temporal bones were collected and immediately fixed in 2.5% glutaraldehyde (Sigma-Aldrich, G5882) for 24 h and then in 1% OsO4 (Beijing

Zhongxingbairui Technology) for 2h, then dehydrated in ethanol, dried, and then coated with gold. For SEM, samples were mounted on stubs, and sputter coated with gold (Cressington, 108). A scanning electron microscope (FEI Quanta 200) operating at 10 kV was used to take images of the hair bundles. For TEM, the sample further penetrated with graded propylene oxide (Macklin Biochemical, P816084) series and gradually polymerized in araldite. The ultra-thin sections made by Leica powertone (Leica, Em UC6) were post-stained with uranyl acetate and lead citrate in turn, and examined by transmission electron microscope (Hitachi, H-7650). All pictures were taken by the electron microscope room of Nanjing Agricultural University.

Real-time quantitative PCR

Samples were dissected to extract total RNA with Trizol reagent (Life, 15596–018) as previously described [41]. Reverse transcription of RNA into cDNA by RevertAid First Strand cDNA Synthesis Kit (Life, K1622), and real-time quantitative PCR (real-time qPCR) was performed by using the FastStart Universal SYBR Green Master (ROX) kit (Roche, 17747200) on Real-Time PCR System (Thermo Fisher Scientific) to quantify the levels of gene expression. The condition of qPCR was as follows: an initial denaturing step: 15 s at 95°C, then followed by 38 cycles of denaturation step: 15 s at 95°C, then followed by annealing step: 60 s at 60°C, and 20 s extension at 72°C. Gapdh was used as the reference gene and used to normalize the mRNA expression data. Using the comparative cycle threshold ($\Delta\Delta C_t$) method to calculate the result. The primers of qPCR are shown in [S1 Table](#).

Western blotting

The basilar membranes of neonatal mice (P0–P7) and the temporal bones of mice older than P7 were dissected, and homogenized in ice-cold RIPA lysis buffer (Beyotime, P0013B) by using tissue homogenizer (Shanghai Jingxin Industrial Development Co., Ltd., JXFSTPRP-48). After centrifuged at 12,000 g for 15 min at 4°C, the supernatant was added with 5X SDS loading buffer (Beyotime, P0015L), separated by 10% or 15% SDS-PAGE, and transferred to an immobilon PVDF membrane (ISEQ00010, Millipore). After blocking with 5% non-fat dried milk in 0.1% PBS-Tween20 for 1 h at RT, the PVDF membrane was incubated with the primary antibody at 4°C overnight. After washing with 0.1% PBS-Tween20 for 5 times per 6 min, the membrane was incubated with HRP-conjugated second antibody (goat anti mouse HRP, M21001, goat anti rabbit HRP, M21002; ABMART) for 1 hour at RT. Signals were detected with the West Femto Trial Kit (Product #34094; Thermo Scientific) on a FluorChem M system (FM0477; ProteinSimple). The primary antibodies were anti-Dync1li1 (abcam, ab157468), anti-Dync1li2 (Proteintech, 18885-1-AP), anti-Dync1li2 (DIC) (Millipore, MAB1618), anti-Dynll1 (DLC) (abcam, ab51603), anti-Rab7 (abcam, ab137029), anti-LC3 (CST, #4108), anti-Calnexin (santa cruz, sc-70481), anti-P-eIF2 α (CST, 3597S), and anti-Gapdh (abcam, ab181602). anti-Dynactin p150 (santa cruz, sc-135890). anti-RILP (Abcam, ab140188)

Cell culture and cell transfection

HEI-OC1 cells were cultured at 37°C with 10% CO₂ in DMEM containing 10% FBS (Pansera, #P30-2602) and 100 IU/ml penicillin (Sigma-Aldrich, A0166). The cells were digested by 0.25% trypsin/EDTA (Life Technologies, #25200056) and then subcultured at 75–80% confluency. When the cells grew to a suitable density, Lipofectamine 2000 Transfection Reagent (Invitrogen, #11668027) was used to transfect plasmids into cells according to the manufacturer's instructions. The shNC-GFP and shDync1li1-GFP plasmids were generated by OBiO

Technology Corp., Ltd. The siNC and siDync1li1 siRNA (5'-CCAGUGCUCGUAGUCU-GUATT-3'; 5'-GACAGAGGUGACAGU GUUGTT-3') were generated by Shanghai GenePharma Company. The shNC-GFP plasmid and siNC siRNA were used as the negative control, and the shDync1li1-GFP (AGTATGGCGCAGCGCTGATTT) plasmid and siDync1li1 siRNA were used to knock down Dync1li1 in HEI-OC1 cells (House Ear Institute-Organ of Corti 1, a cochlear HC-like cell line). The LC3-RFP plasmid, which was a kind gift from Prof. Zheng Ying (Soochow University, Jiang Su, China) [42–45], was used to label LC3⁺ autophagic vacuoles. The RFP-GFP-LC3 plasmid was purchased from Hanbio Biotechnology (Lot. No. TSB005062-1).

Data quantification and statistical analysis

The number of myo7a⁺ outer HCs (OHCs) and inner HCs (IHCs) per 100 μm were counted in the apical, middle, and basal turns of the cochlea. For synapse counting, Z-projection was performed to project multiple slides of a Z-stack image onto a single layer, and the numbers of Ctbp2⁺ and PSD95⁺ puncta were counted in the apical, middle, and basal turn of the cochlea per 100 μm using the ImageJ software (S3 Fig). For HEI-OC1 cells, all of the LC3-RFP fluorescent puncta were counted in each HEI-OC 1 cell, and over 50 GFP-shRNA/LC3-RFP double-positive cells were counted. For each experiment, at least three independent experiments were performed. GraphPad Prism 7 software was used to analyze the data and presented as means \pm standard errors of the means. A two-tailed, unpaired Student's t-tests were performed to analyze the data, and $p < 0.05$ was considered statistically significant.

Results

Dync1li1 is expressed in cochlear HCs in both neonatal and adult mice

RT-PCR showed that *Dync1li1* mRNA was highly expressed in postnatal day 3 (P3) mouse cochlea and in the HEI-OC1 cell line (Fig 1A). Dync1li1 protein was also detected by western blotting in P3 cochlea (Fig 1B). Next, immunofluorescent staining showed that Dync1li1 was highly expressed in HCs in both whole mount and frozen sections of P3 (newborn) and P30 (adult) mouse cochlea. In addition, we also observed that Dync1li1 is also expressed in other types of cells in the organ of Corti, such as spiral neurons and some of supporting cells (Fig 1C–1E). Fig 1F shows a diagram of the IHC and OHC of cochlea. These results suggested that Dync1li1 is highly expressed in HCs and might play important roles in HCs in both the neonatal and adult cochlea.

Dync1li1 KO leads to progressive HC loss *in vivo*

Next, we showed that *Dync1li1* is indeed knocked out in Dync1li1 KO mice (Figs 2A and S4). We first sacrificed mice from neonatal to adult ages to investigate whether HC number is affected by *Dync1li1* KO. We saw no significant HC loss before P21 in *Dync1li1* KO mice, while slight HC loss could be observed from P21 and HC loss gradually became more and more severe as the mice aged (Figs 2B and S1). Quantification of HC loss showed no significant HC loss in P21 mice, although a few HCs were lost in the basal turn. However, significant OHC loss was seen in the apical, middle, and basal turns of the cochlea in P30 and P60 mice (Fig 2C), while the number of IHCs was not significantly changed (Fig 2D). Immunofluorescent staining and scanning electron microscopy (SEM) both showed that the hair bundles of surviving HCs in *Dync1li1* KO mice had normal morphology (Fig 2E and 2F). Because HCs are important sound-sensing cells, we used auditory brainstem response to detect the hearing ability of *Dync1li1* KO mice. Consistent with the degree of HC loss, the hearing thresholds of

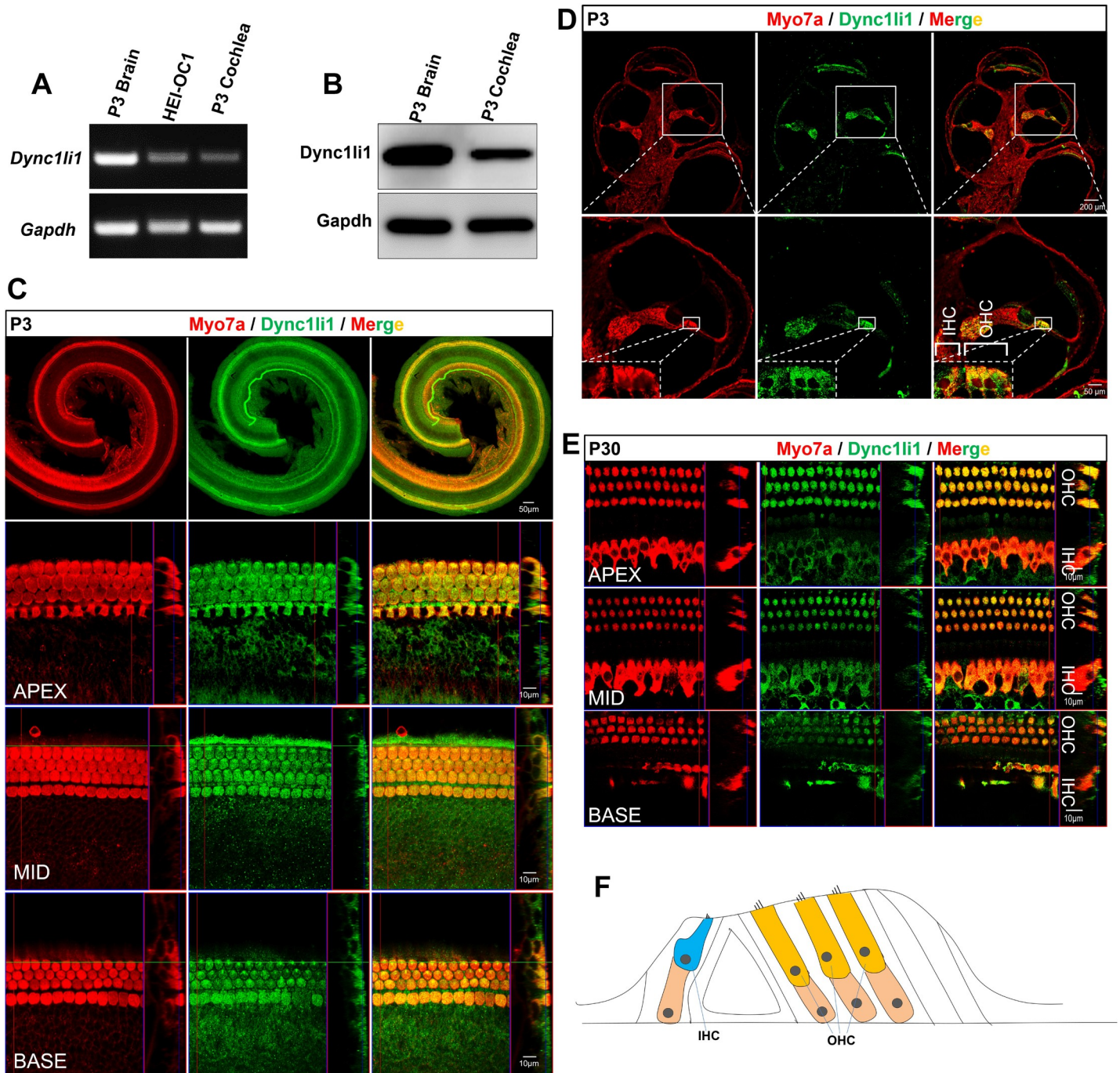


Fig 1. The expression pattern of Dync1li1 in the cochlea of wild-type mice. (A, B) *Dync1li1* mRNA (A) and protein (B) expression in P3 mouse cochlea by RT-PCR and Western blotting, respectively. Brain tissue and the HEI-OC1 cell line were used as the positive controls. (C) Whole mount immunofluorescent staining of Dync1li1 in P3 mouse cochlea. The large square image is a single XY slice, the vertical red line shows the position of the orthogonal slice, which is shown on the right side of each panel, and the blue line on the orthogonal line shows the level of the XY slice on the left. (D) Frozen section immunofluorescent staining of Dync1li1 in P3 mouse cochlea. The white boxes and the dotted lines show enlarged images. (E) Whole mount immunofluorescent staining of Dync1li1 in P30 adult mouse cochlea. For all experiments, scale bars are shown in the figure. (F) A diagram of the IHC and OHC in the cochlea.

<https://doi.org/10.1371/journal.pgen.1010232.g001>

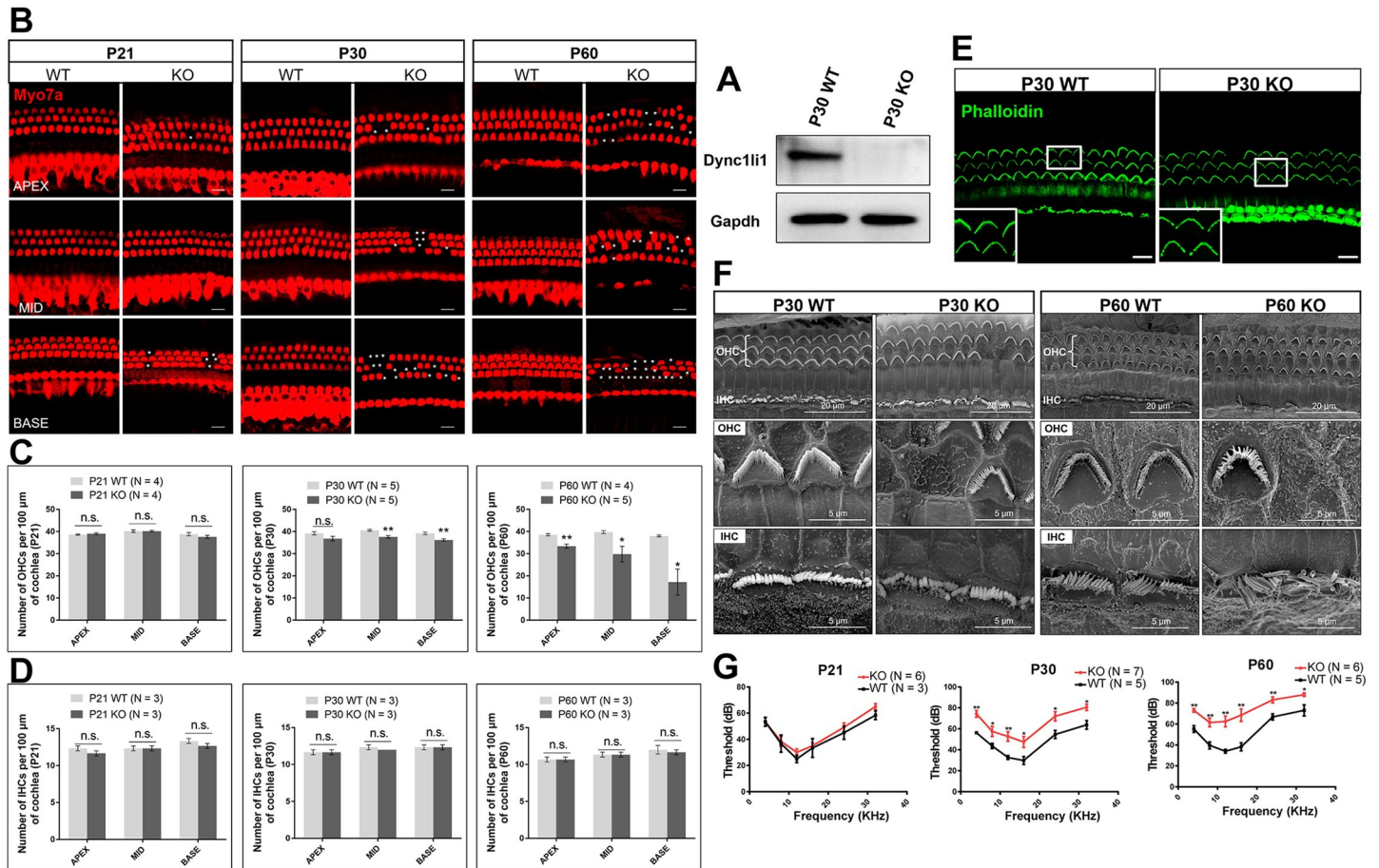


Fig 2. *Dync1li1* KO results in HC loss and hearing loss in adult mice. (A) Western blotting of *Dync1li1* in P30 mouse cochlea. *Gapdh* was used as the internal reference. (B) OHC loss (indicated by asterisks) is seen in the apical (APEX), middle (MID), and basal (BASE) turns of P21, P30, and P60 *Dync1li1* KO and wild-type (WT) mice cochlea. *Myo7a* (red) was used as the HC marker. (C, D) Quantification of the OHCs (C) and IHCs (D) in the apical, middle, and basal turns of P21, P30, and P60 *Dync1li1* KO and WT mice cochlea. (E, F) Hair bundles were observed by immunofluorescent staining of phalloidin (E) and scanning electron microscopy (F). The enlarged images in the white box in (E) is shown in the lower left corner. (G) The ABR hearing test of *Dync1li1* KO mice and control mice at P21, P30, and P60. For all experiments, scale bars and N number are shown in the figure. * $p < 0.05$, ** $p < 0.01$, n.s. not significant.

<https://doi.org/10.1371/journal.pgen.1010232.g002>

the *Dync1li1* KO mice were not affected at P21 but were significantly increased at P30 and P60 (Fig 2G). Together these results suggest that *Dync1li1* is highly expressed in HCs and that its deletion results in progressive HC loss and hearing loss in adult mice, and thus that *Dync1li1* plays important roles in HC survival.

TUNEL signals, which are indicative of apoptosis, were observed in HCs of both P21 and P30 *Dync1li1* KO mice, but not in the control group (Fig 3A). Real-time qPCR results also showed that the expression of apoptosis-related genes, such as *Aparf* and *Caspase3*, were significantly upregulated in the *Dync1li1* KO mouse cochlea (Fig 3B). Together, these results indicate that HC loss in *Dync1li1* KO mice was due to HC apoptosis.

Dync1li1 KO decrease the stability of Dynein complex in HCs

Because *Dync1li1* is an important part of the dynein complex, which is crucial in all eukaryotic cells for transporting a variety of essential cargoes toward the minus end of microtubules (also called retrograde transport), we speculated that HC apoptosis caused by *Dync1li1* KO might be related to impaired retrograde transportation. Thus, we first detected the expression of other

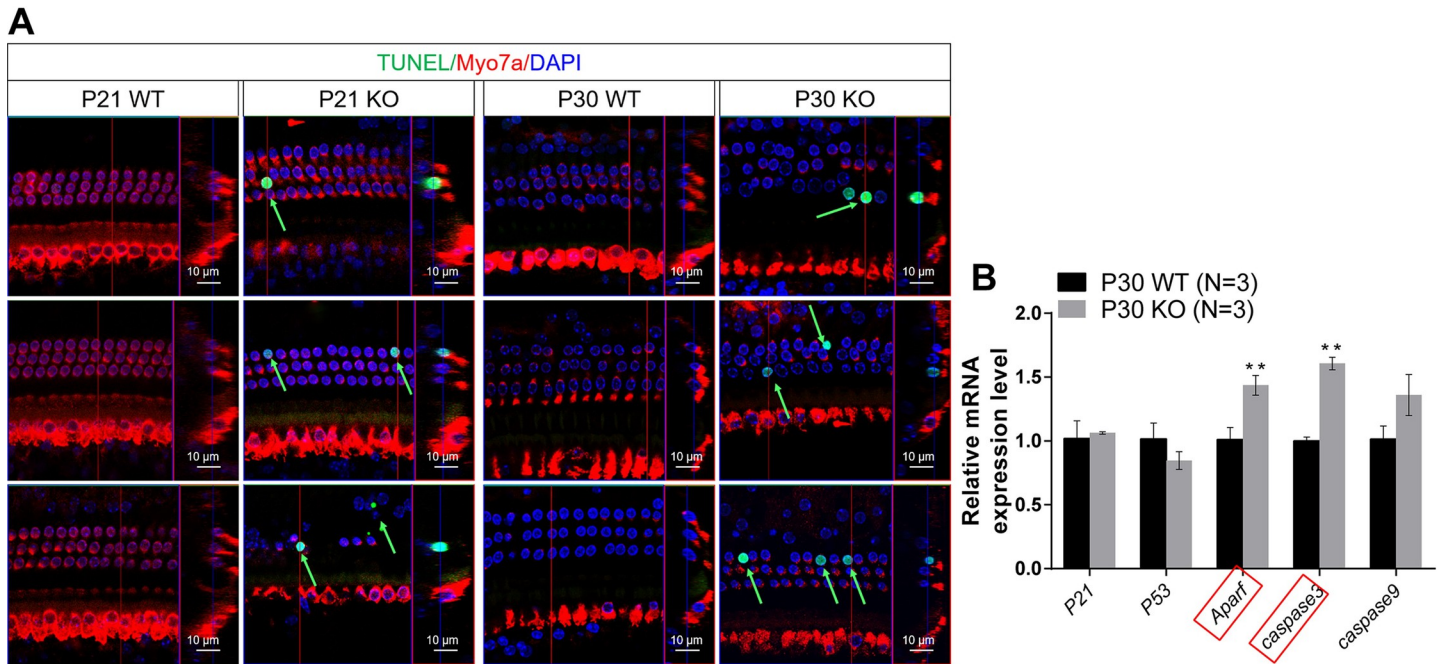


Fig 3. Apoptosis analysis by TUNEL assay in the cochlea of *Dync1li1* KO mice at P21 and P30. (A) TUNEL assay of P21 and P30 *Dync1li1* KO mice and WT control mice. Myo7a and DAPI were used as HC and nuclear markers, respectively. Apoptotic cells are indicated by green arrows. (B) Quantification of the mRNA expression of apoptosis related genes in the cochlea of P30 *Dync1li1* KO mice and the control mice by qPCR. Red boxes indicate the genes with significant expression differences. For all experiments, scale bars and N number are shown in the figure. ** $p < 0.01$.

<https://doi.org/10.1371/journal.pgen.1010232.g003>

components of the dynein complex to determine the stability of dynein. The mRNA levels of *Dync1h1* (DHC), *Dync1i1* (one of the DIC genes), and *Dync1l1* (one of the DLC genes) were all significantly downregulated in P60 *Dync1li1* KO mouse cochlea (Fig 4A), and the protein level of Dync1i1/2 (DIC) and Dync1l1 (DLC) were also significantly downregulated, with Dync1i1/2 being the most pronounced and the expression of Dync1li2 was not significantly changed in P30 *Dync1li1* KO mice (Fig 4B and 4C). We then used TEM to explore the effects on transport-related organelles in cochlear HCs, such as the structure of the endoplasmic reticulum (ER) and the Golgi apparatus, and we found that the number of lamellae per Golgi was significantly reduced in *Dync1li1* KO OHCs compared to the control group and that the Golgi apparatus was thinner in the *Dync1li1* KO OHCs (Fig 4D–4F). Together, these results indicate that deletion of *Dync1li1* leads to unstable dynein complexes and to decreased stacks of Golgi apparatus in cochlear OHCs.

HC apoptosis caused by *Dync1li1* KO is due to impaired transportation of autophagosomes to lysosomes. Considering that dynein plays crucial roles during the autophagic process (Fig 5D) and that autophagy is involved in apoptosis [46], we hypothesized that the HC apoptosis caused by *Dync1li1* KO is due to impaired transportation of autophagosomes to lysosomes. To test this, we first detected the LC3 signal (autophagic vacuoles marker) in HCs of P60 *Dync1li1*^{-/-}LC3-GFP mice and found significantly more LC3-positive puncta in the OHCs of *Dync1li1*^{-/-}LC3-GFP mice compared to the LC3-GFP-only control mice (Fig 5A and 5B). Western blotting showed that the LC3 and Sqstm1/p62 protein level were upregulated in P60 *Dync1li1* KO mouse cochlea, suggesting that autophagic vacuoles were aggregated in the HCs (Fig 5C). Moreover, Rab7, an adaptor protein during the maturation of autolysosomes [47,48], was also upregulated in the cochlea of P60 *Dync1li1* KO mice (Fig 5C), which indicated that

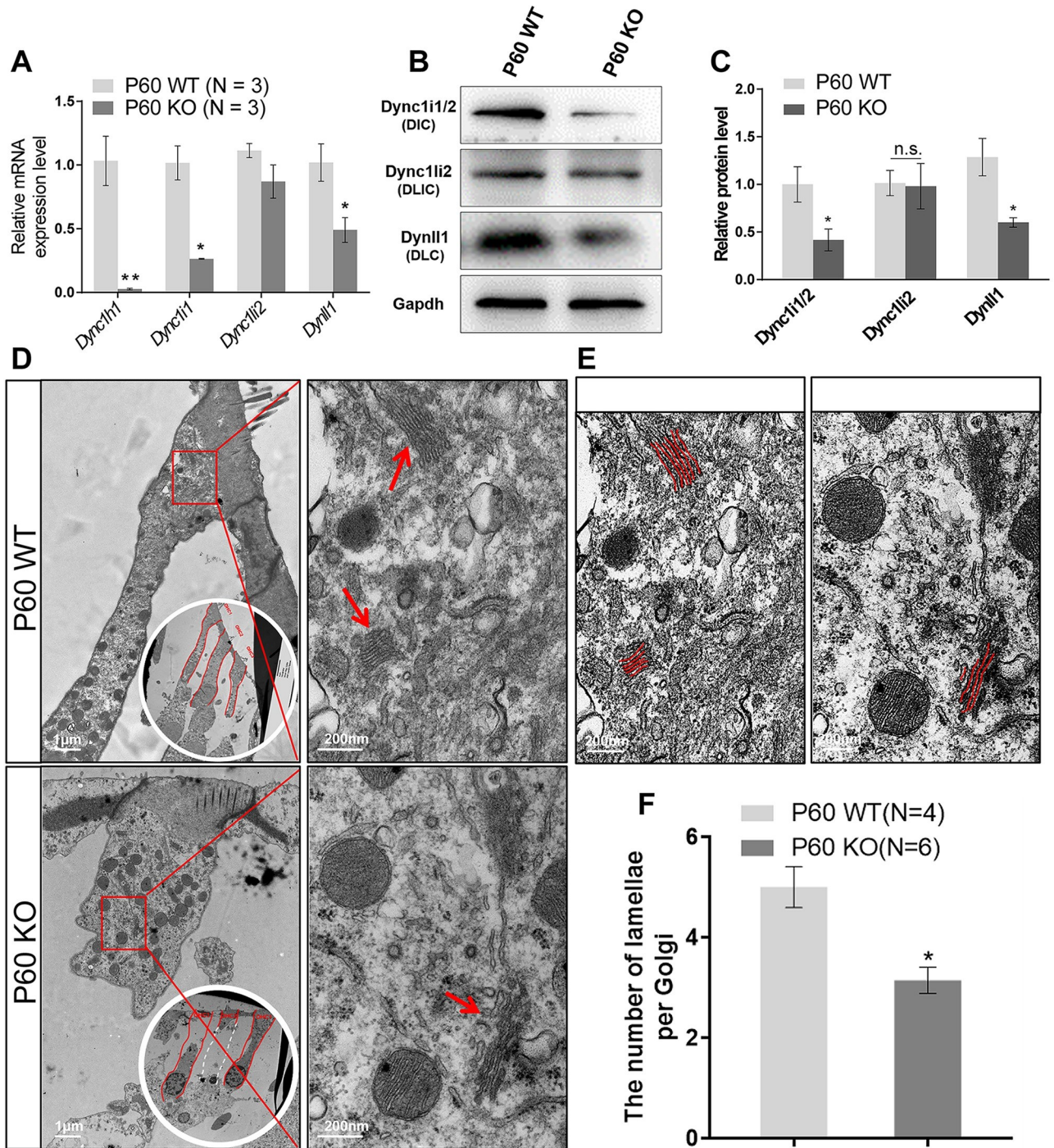


Fig 4. Dync1li1 deficiency affect the integrity of Dynein complex and Golgi apparatus. (A) Quantification of the mRNA expression of important subunits in dynein complex (*Dync1h1*, *Dync1i1*, and *Dynll1*) in P60 *Dync1li1* KO and the control mice by qPCR. N = 3. N refers to 3 independent qPCR experiments were performed. (B, C) Western blotting (B) and quantification of the western blotting (C) of the Dynein subunit in the cochlea of P60 *Dync1li1* KO mice. Gapdh was used as the internal reference. N is indicated in the figure. (D, E) TEM of OHCs in P60 *Dync1li1* KO and control mice. The Golgi apparatus is indicated by red arrows in (D) and red lines in (E). (F) Quantification of the number of lamellae per Golgi. For all experiments, scale bars are shown on the figure and N is indicated in the figure. *p < 0.05, ***p < 0.001.

<https://doi.org/10.1371/journal.pgen.1010232.g004>

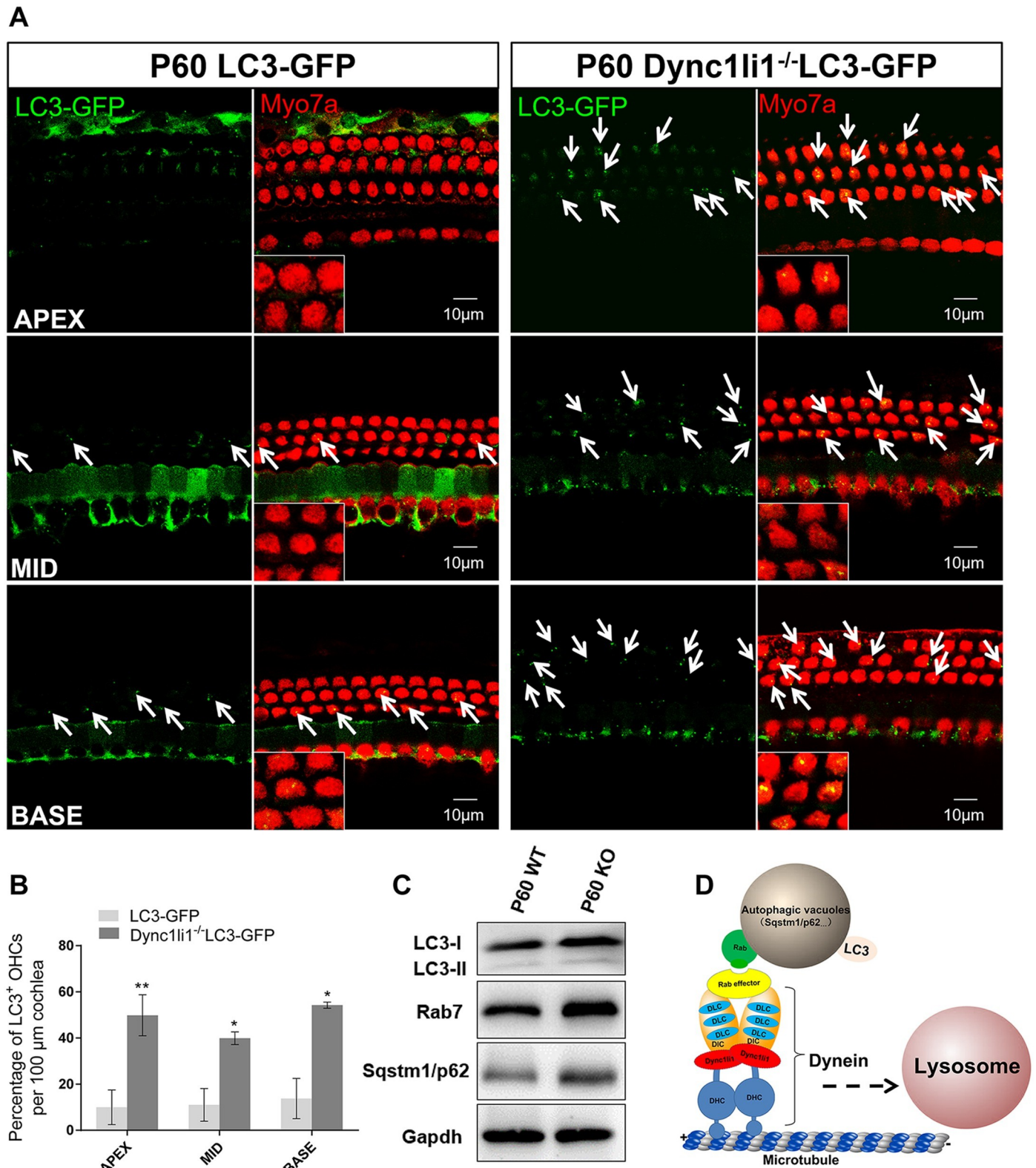


Fig 5. *Dync1li1* deficiency induced the accumulation of autophagosomes vacuoles in HCs. (A) Immunofluorescence of LC3 (green puncta, indicated by white arrows) in HCs of P60 *Dync1li1*^{-/-}LC3-GFP mice and control mice. *Myo7a* was used as HC marker. The enlarged images are shown in the lower left corner. (B) Quantification of the number of LC3⁺ OHCs. N = 3. (C) Western blotting of the LC3 (LC3-I, 16 kDa; LC3-II, 14 kDa), Rab7, and Sqstm1/p62 in the cochlea. Gapdh

was used as the internal reference. (D) Schematic of the role of dynein in mediating autophagosome–lysosome fusion. Rab links autophagosomes to dynein to mediate microtubule-dependent minus-end-directed transportation towards the lysosome. For all experiments, scale bars are shown in the figure. * $p < 0.05$, ** $p < 0.01$.

<https://doi.org/10.1371/journal.pgen.1010232.g005>

newly formed autophagosomes (with Rab7 on their surface) could not be transported to lysosomes for degradation and thus had accumulated in the HCs.

Next, we verified these results in the HC-like HEI-OC1 cell line [49]. We used shRNA to knock down *Dync1li1* in the HEI-OC1 cell line and confirmed the KD efficiency (Fig 6A and 6B). We then transfected the LC3-RFP plasmid into HEI-OC1 cells and quantified the LC3 puncta, and we found that the number of LC3 puncta was significantly increased in the *Dync1li1* KD group at both 24 h and 36 h after transfection compared to the controls (Fig 6C and 6D).

RFP-GFP-LC3 is a tool plasmid for detecting the level of autophagy in cells as illustrated in Fig 6E [50]. There are two fluorescent protein, red RFP and green GFP, expressed as a fusion protein with LC3, in which GFP is a pH sensitive protein. When in the autophagic vacuoles with a neutral pH (autophagosome), RFP and GFP both show fluorescent signal, and thus the LC3 dots are yellow (GFP+/RFP+). When in the autophagic vacuoles with an acidic pH (autolysosome), GFP cannot show fluorescent signal and only RFP can show red fluorescent signal, and thus the LC3 dots are red. Therefore, we can use this plasmid to measure autophagic flux in the *Dync1li1* KD group and the control group. And we found that in *Dync1li1* KD OC1 cells, the number of autophagosomes (GFP+/RFP+) were significantly more than that in the control group, while the number of autolysosomes (GFP-/RFP+) was less than that in the control group (Fig 6F and 6G). These data suggested that *Dync1li1* KD led to accumulation of autophagosomes which cannot be eliminated by transporting to lysosomes to form autolysosomes. Moreover, we also found that the protein level of Dync1li1/2 (DIC) and Dync1li1 (DLC) were also significantly down regulated, the expression of Dync1li2 was not changed, and the protein level of LC3 and Sqstm1/p62 were up regulated in *Dync1li1* KD group (Fig 6H and 6I). These results are consistent with the changes in protein level in *Dync1li1* KO mouse cochlea. Therefore, we conclude that knock down of *Dync1li1* in vitro led to impaired transportation of autophagosomes to lysosomes and to abnormal accumulation of autophagosomes in HC-like HEI-OC1 cells.

In summary, the mechanisms we identified are shown in Fig 7. Under normal conditions, late autophagosomes with harmful substances produced in HCs are transported by dynein to be fused with lysosomes and form autolysosomes for subsequent degradation, thereby maintaining cell homeostasis. When Dync1li1 is defective or missing, the dynein complex becomes unstable and cannot effectively transport late autophagosomes to lysosome for degradation, which leads to the accumulation of these autophagosomes with harmful substances. This disruption in cell homeostasis triggers HC apoptosis and thus leads to hearing loss.

Discussion

Dynein plays critical roles in the central nervous system through its effects on nuclear migration and retrograde transport of various cargos [51]. In this study, we found that one member of the dynein complex, Dync1li1, was highly expressed in cochlear HCs, and *Dync1li1* KO mice showed progressive hearing loss along with early onset of HC apoptosis. Further study revealed that Dync1li1 deletion decreased the expression level of other members of dynein complex, including the DHC, DIC, and DLC, which further reduced the number of lamellae in the Golgi apparatus and led to the accumulation of autophagosomes in HCs. Together our data suggest that the unstable dynein complex caused by *Dync1li1* KO affects Golgi-related

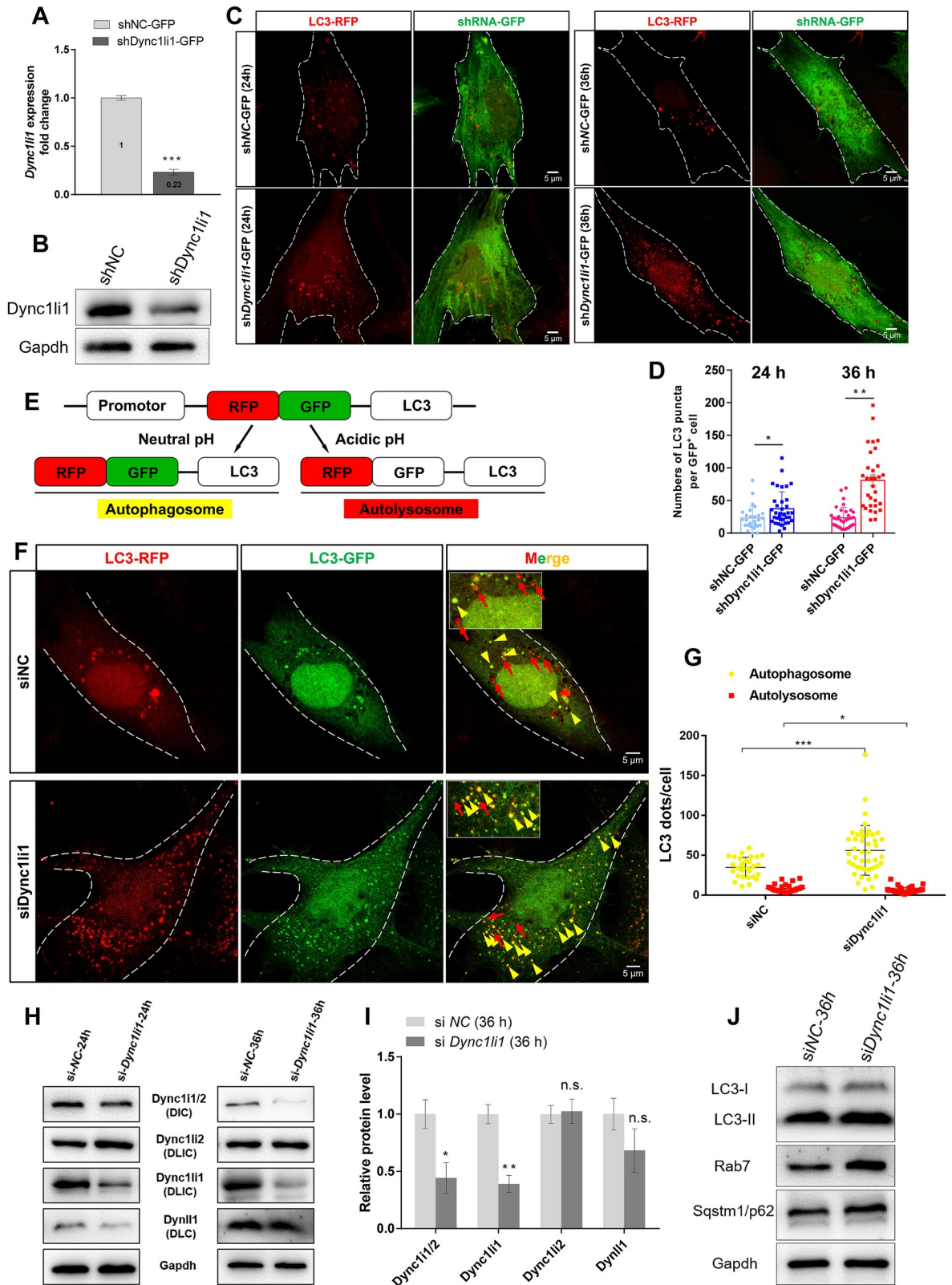


Fig 6. Accumulation of autophagosomes in *Dync1li1* KD HEI-OC1 cells. (A, B) OC1 Cells were transfected with sh*Dync1li1*-GFP shRNA, and qPCR analysis (A) and Western blotting (B) were used to test the knockdown efficiency of *Dync1li1*. shNC-GFP was used as control shRNA. The cells were harvest after 36h transfection. (C, D) shNC-GFP and sh*Dync1li1*-GFP were cotransfected with LC3-RFP

plasmids into OC1 cells for 24 h and 36 h, respectively. Red dots in (C) indicate the LC3 puncta (autophagic vacuoles), which were quantified in (D). (E) Schematic of the working principle of the RFP-GFP-LC3 plasmid. In a neutral environment (autophagosome), LC3 is expressed with both GFP and RFP fluorescent proteins, and thus the autophagosome dots (RFP⁺GFP⁺) are yellow. In an acidic environment (autolysosome), GFP fluorescence is quenched, and thus the autolysosome dots (RFP⁺) are red. (F, G) siNC and siDync1li1 siRNA were cotransfected with RFP-GFP-LC3 plasmid for 36 h. Yellow arrow heads and red arrows in (F) indicate the autophagosomes (yellow dots) and the autolysosomes (red dots), respectively. The enlarged images are shown in the upper left in (F). The number of autophagosomes and autolysosomes in the *Dync1li1* KD cells and the control cells were quantified in (G). (H, I) siNC and siDync1li1 siRNA were transfected for 24 h and 36 h, respectively. Western blotting (H) and quantification of Dynein subunit proteins after siRNA transfection. Quantification of protein expression levels at 36 h after siRNA transfection (I). (J) Western blotting of LC3, Sqstm1/p62 and Rab7 at 36 h after siRNA transfection. For all experiments, scale bars are shown in the figure. **p* < 0.05, ***p* < 0.01, n.s. not significant.

<https://doi.org/10.1371/journal.pgen.1010232.g006>

transport and the transport of autophagosomes to lysosomes and that this ultimately results in HC apoptosis in the cochlea.

The cilia of HCs (called HC bundles) show a highly ordered arrangement that makes them highly sensitive to vibration of the fluid environment, and the planar cell polarity (PCP) of HC bundles is essential for hearing function [52–55]. It is reported that *Dync1li1* knockout mice show deficient ciliogenesis of photoreceptors [20]. Here we found that *Dync1li1* is highly expressed in auditory HC cytoplasm, rather than in HC bundles, in both neonatal and adult mouse cochlea. *Dync1li1* KO mice showed progressive HC loss and hearing loss at all frequencies, but no changes were observed in the morphology or PCP of HC bundles. These results indicated that the function of *Dync1li1* in HCs was not involved in the formation or PCP of the hair bundles.

The TUNEL assay showed that HC loss caused by *Dync1li1* deficiency is due to early onset of HC apoptosis. Previous study showed that separation of DLIC from the dynein complex result in unstable DHC in vertebrate [7]. In the mouse retina, loss of *Dync1li1* reduced the protein levels of DHCDIC and DLC and therefore impair the transport ability of dynein [20]. Consistent with previous reports, here we also found that deletion of *Dync1li1* led to decreased expression of the DHC, DIC, and DLC in mouse cochlea and thus caused the destabilization of the dynein complex in cochlear HCs. In the photoreceptor cells, LIC1 deletion also increase dynactin P150 (a dynein adaptor linking dynein to cargoes) protein expression [20], we also investigate the protein level of P150 in the KO *Dync1li1* mouse cochlea (S2C Fig).

Considering that dynein is involved in maintaining the architecture of the ERGIC (ER-Golgi intermediate compartment) and that inhibition of dynein leads to fragmentation and dispersion of the Golgi apparatus [15,56–58], we also investigated the effects of *Dync1li1* deletion on the morphology of the ER and Golgi apparatus in HCs. Our TEM data showed that the lamellae of the Golgi apparatus were thinner in *Dync1li1* KO OHCs, which suggested that *Dync1li1* deletion led to disorganization of transport processes in the Golgi apparatus. We also measured the ER stress level by measuring the protein level of Calnexin and P-eIF2 α , and we found that neither of them were significantly changed (S2A and S2B Fig). Since RILP is also an important adapter for dynein, we investigated the expression of RILP in the KO *Dync1li1* mouse cochlea. Interestingly, we found that the protein level of RILP was not significantly changed (S2D Fig). We also investigated the location and the number of auditory ribbon synapses in *Dync1li1* KO mice, but we did not observe any abnormalities. Both the location and the number of ribbon synapses were normal in HCs of *Dync1li1* KO mice (S3 Fig), which indicated that *Dync1li1* deficiency did not affect the formation of ribbon synapses.

Accumulating studies have shown that the dynein complex is involved in autophagic processes and dynein-dependent retrograde transport of autophagic vacuoles is essential for the survival of neurons [37,38,59–61]. Dynein inhibition impair the process of clearance of aggregate-prone proteins in the drosophila and mouse model of Huntington's disease [35]. The mutation of dynein weaken the clearance of mutant huntingtin fragments by cross the

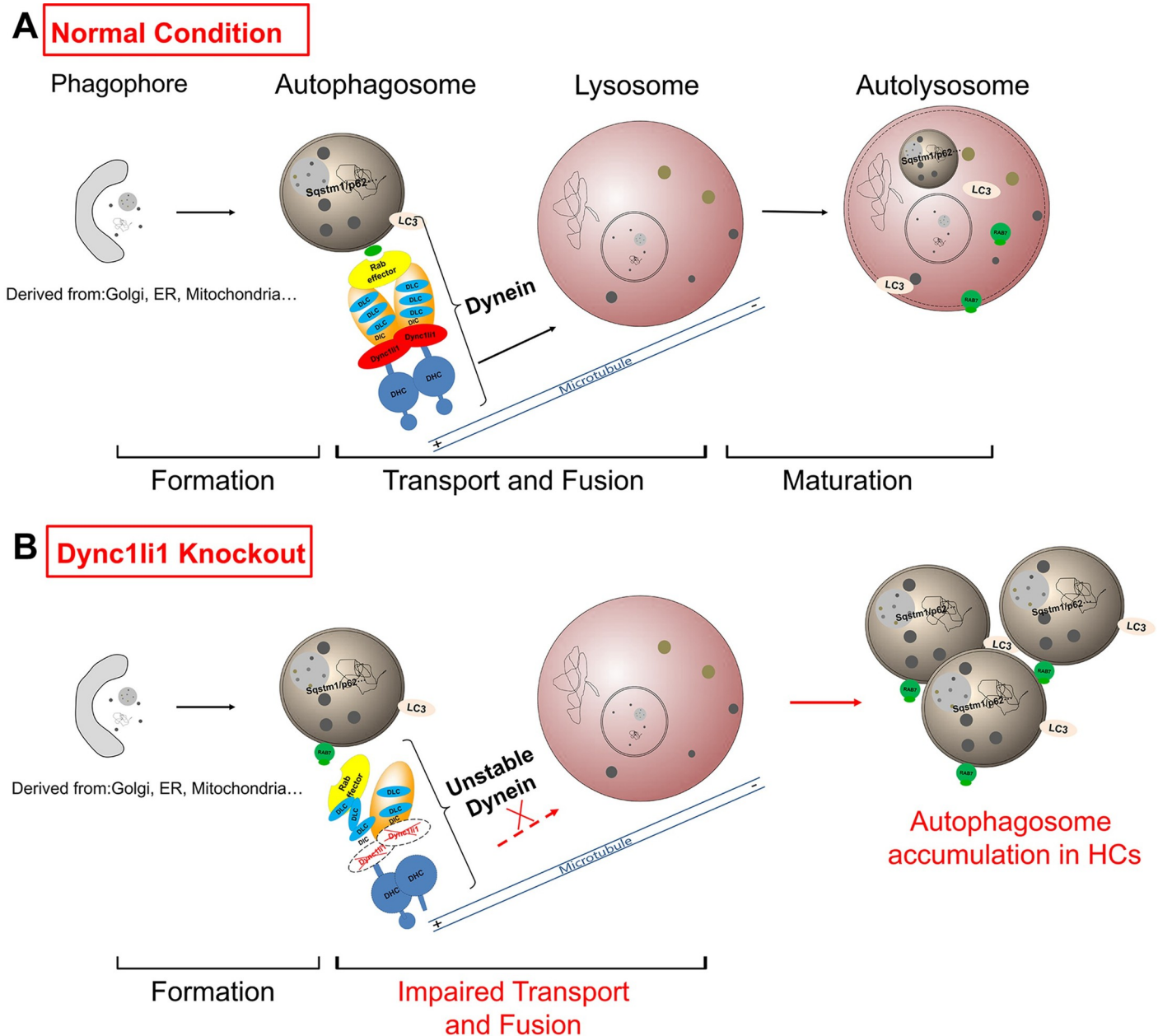


Fig 7. Working model of dynein-dependent autolysosome clearance in cochlear HCs. (A) Under normal conditions, phagophores (derived from the ER, Golgi, mitochondria, etc.) expand and form late autophagosomes, which bind to the dynein complex through Rab7. Late autophagosomes, with both LC3 and Rab7 expressed on their membranes, are transported by dynein along microtubules to lysosomes to form autolysosomes and to be digested. This autophagic flux maintains homeostasis in HCs. (B) When *Dync1li1* is knocked out in cochlear HCs, the fusion of late autophagosomes with lysosomes is impaired by the unstable dynein complex. Therefore, large numbers of late autophagosomes are accumulated in the HCs, which disrupts normal autophagic flux and leads to HC apoptosis.

<https://doi.org/10.1371/journal.pgen.1010232.g007>

HdhHD mice (mouse model of Huntington disease [62]) with *Dnchc1Loa* (ethylnitrosourea-induced missense mutation in the dynein heavy chain 1 [63]), and the level of LC3-II expression in *Hdh+/+ Dnchc1Loa/+* mice was increased [35].

Basal autophagy is important for homeostasis in postmitotic cells [64,65]. In the inner ear, basal autophagic flux can be detected in cochlear HCs and is essential for hearing in mice [66,67], and autophagy-deficient mice show impaired biogenesis of otoconia [68]. However,

there is no research about the relation between dynein and autophagy in cochlear HCs. In our study, we observed that the endogenous LC3 puncta were significantly increased in both HCs and HC-like HEI-OC1 cells after *Dync1li1* KO or KD, which suggested that without dynein the process of autophagosome clearance was abnormal and that this led to the accumulation of autophagosomes in HCs that in turn triggered apoptosis in HCs and subsequent hearing loss.

Many studies have shown that Rab7 is required for the complete autophagic flux and that it regulates the process of autophagosome-lysosome fusion [69,70]. These studies indicated the strong interaction between dynein and Rab7 in the process of late autophagosome-lysosome fusion. Here, our results showed that both the protein level of Rab7 and LC3 were significantly increased in cochlear HCs of *Dync1li1* KO mice and *Dync1li1* KD HEI-OC1 cells *in vitro*, which suggested that late autophagosomes accumulated in *Dync1li1*-deficient cells. Therefore, we speculated that deletion of *Dync1li1* impaired the transportation of late autophagosomes to lysosomes, such that LC3+ autophagosomes could not be cleared and therefore accumulated in the HCs. However, it is worth noting that Rab7 is also a marker of late endosomes [71] and that Rab7 is required for mitophagosome formation by regulating phagophore transport [72,73]. Therefore, in future work we will further explore the effects of *Dync1li1* deletion on other Rab7-mediated transport processes in the mouse cochlea.

In summary, we have identified new roles for *Dync1li1* in maintaining the survival of mouse cochlear HCs. We show that *Dync1li1* KO leads to destabilization of the dynein complex and that this results in impaired transport of late autophagosomes to lysosomes. Therefore, LC3⁺ autophagosomes cannot be cleared and thus accumulate in HCs, which leads to HC apoptosis and hearing loss in adult mice.

Supporting information

S1 Fig. No HC loss is observed in the cochleae of *Dync1li1* KO mice at P1 and P14. (A, B) Immunofluorescent staining of Myo7a and Phalloidin in P1 (A) and P14 (B) *Dync1li1* KO mice and WT control mice cochleae, respectively. Myo7a was used as HC marker. Phalloidin was used as HC bundle marker. (C, D) Quantification of OHC (C) and IHC (D) number in the apical (APEX), middle (MID), and basal (BASE) turns of P1 *Dync1li1* KO and control mice cochleae. (E, F) Quantification of OHC (E) and IHC (F) number in the apical (APEX), middle (MID), and basal (BASE) turns of P14 *Dync1li1* KO and control mice cochleae. For all experiments, scale bar are shown on the figure, N is indicated in the figure, n.s. not significant. (TIF)

S2 Fig. The analysis protein level of expression of ER stress-related proteins, P150 and RILP in *Dync1li1* KO mice at P30. (A, B,C,D) Western blotting of Calnexin (A), P-eIF2 α (B), P150 (C) and RILP (D) in the cochleae of P30 *Dync1li1* KO mice and WT mice. Calnexin was used as the ER marker and P-eIF2 α was used as the ER stress marker. Gapdh was used as the internal control. (TIF)

S3 Fig. The ribbon synapses of IHCs in P21 *Dync1li1* KO mice. (A) Immunofluorescent staining of Ctbp2 and PSD95 in P21 *Dync1li1* KO mice and WT control mice IHCs, respectively. Images were taken from the MID turn of the cochleae. The enlarged image in the white box is shown in the lower right corner. Ctbp2 was used as presynaptic marker. PSD95 was used as postsynaptic marker. (B) Quantification of the number of synapses from MID turn of *Dync1li1* KO and WT mice. For all experiments, scale bars are shown on the figure, n.s. not significant. (TIF)

S4 Fig. The full blot of LIC in Fig 2A.

(TIF)

S1 Table. Primers for real-time qPCR detection and relative quantification of gene expression in mouse.

(DOCX)

S1 Note. Abbreviations.

(DOCX)

Acknowledgments

We thank Prof. Wufan Tao from Fudan University for providing Dync1li1 KO transgenic mice. We thank Prof. Zheng Ying from Soochow University for providing LC3-RFP plasmid.

Author Contributions

Conceptualization: Yuan Zhang, Shasha Zhang, Xiaoyun Qian, Xia Gao, Renjie Chai.

Data curation: Yuan Zhang, Shasha Zhang, Han Zhou, Xiangyu Ma, Leilei Wu, Mengyao Tian, Siyu Li.

Formal analysis: Yuan Zhang, Shasha Zhang, Renjie Chai.

Funding acquisition: Xiaoyun Qian, Renjie Chai.

Investigation: Yuan Zhang, Shasha Zhang.

Methodology: Yuan Zhang, Shasha Zhang.

Project administration: Yuan Zhang.

Resources: Yuan Zhang.

Software: Yuan Zhang, Han Zhou, Xiangyu Ma, Leilei Wu.

Validation: Yuan Zhang, Shasha Zhang, Siyu Li, Xiaoyun Qian, Xia Gao, Renjie Chai.

Visualization: Yuan Zhang, Mengyao Tian, Xia Gao.

Writing – original draft: Yuan Zhang, Shasha Zhang, Xiaoyun Qian, Xia Gao.

Writing – review & editing: Shasha Zhang, Xia Gao, Renjie Chai.

References

1. Deafness and hearing loss. 2020; Available from: <https://www.who.int/news-room/fact-sheets/detail/deafness-and-hearing-loss>.
2. Dror A.A. and Avraham K.B., Hearing Loss: Mechanisms Revealed by Genetics and Cell Biology. *Annual Review of Genetics*. 2009; 43(1): p. 411–437. <https://doi.org/10.1146/annurev-genet-102108-134135> PMID: 19694516
3. Bhabha G., Johnson G.T., Schroeder C.M., and Vale R.D., How Dynein Moves Along Microtubules. *Trends in biochemical sciences*. 2016; 41(1). <https://doi.org/10.1016/j.tibs.2015.11.004> PMID: 26678005
4. Reck-Peterson S.L., Redwine W.B., Vale R.D., and Carter A.P. The cytoplasmic dynein transport machinery and its many cargoes. *Nat Rev Mol Cell Biol*. 2018; 19(6): p. 382–398. <https://doi.org/10.1038/s41580-018-0004-3> PMID: 29662141
5. Belyy V., Hendel N.L., Chien A., and Yildiz A. Cytoplasmic dynein transports cargoes via load-sharing between the heads. *Nature communications*. 2014; 5: p. 5544. <https://doi.org/10.1038/ncomms6544> PMID: 25424027

6. Williams J.C., Roulhac P.L., Roy A.G., Vallee R.B., Fitzgerald M.C., and Hendrickson W.A. Structural and thermodynamic characterization of a cytoplasmic dynein light chain-intermediate chain complex. *Proceedings of the National Academy of Sciences of the United States of America*. 2007; 104(24): p. 10028–10033. <https://doi.org/10.1073/pnas.0703614104> PMID: 17551010
7. King S.J., Bonilla M., Rodgers M.E., and Schroer T.A. Subunit organization in cytoplasmic dynein sub-complexes. *Protein science: a publication of the Protein Society*, 2002; 11(5): p. 1239–1250. <https://doi.org/10.1110/ps.2520102> PMID: 11967380
8. Pfister K.K. Dynein cargo gets its groove back. *Structure (London, England: 1993)*, 2005; 13(2): p. 172–173. <https://doi.org/10.1016/j.str.2005.01.003> PMID: 15698561
9. Celestino R., Henen M.A., Gama J.B., Carvalho C., McCabe M., Barbosa D.J., et al. A transient helix in the disordered region of dynein light intermediate chain links the motor to structurally diverse adaptors for cargo transport. *PLoS biology*. 2019; 17(1): p. e3000100. <https://doi.org/10.1371/journal.pbio.3000100> PMID: 30615611
10. Pfister K.K., Shah P.R., Hummerich H., Russ A., Cotton J., Annuar A.A., et al. Genetic analysis of the cytoplasmic dynein subunit families. *PLoS genetics*. 2006; 2(1): p. e1. <https://doi.org/10.1371/journal.pgen.0020001> PMID: 16440056
11. Tynan S.H., Gee M.A., and Vallee R.B. Distinct but overlapping sites within the cytoplasmic dynein heavy chain for dimerization and for intermediate chain and light intermediate chain binding. *The Journal of biological chemistry*. 2000; 275(42): p. 32769–32774. <https://doi.org/10.1074/jbc.M001537200> PMID: 10893223
12. Schroeder C.M., Ostrem J.M.L., Hertz N.T., and Vale R.D. A Ras-like domain in the light intermediate chain bridges the dynein motor to a cargo-binding region. *eLife*, 2014; 3: p. e03351. <https://doi.org/10.7554/eLife.03351> PMID: 25272277
13. Lee I.-G., Olenick M.A., Boczkowska M., Franzini-Armstrong C., Holzbaur E.L.F., and Dominguez R. A conserved interaction of the dynein light intermediate chain with dynein-dynactin effectors necessary for processivity. *Nature communications*. 2018; 9(1): p. 986. <https://doi.org/10.1038/s41467-018-03412-8> PMID: 29515126
14. Mische S., He Y., Ma L., Li M., Serr M., and Hays T.S. Dynein light intermediate chain: an essential subunit that contributes to spindle checkpoint inactivation. *Molecular biology of the cell*. 2008; 19(11): p. 4918–4929. <https://doi.org/10.1091/mbc.e08-05-0483> PMID: 18799620
15. Palmer K.J., Hughes H., and Stephens D.J. Specificity of cytoplasmic dynein subunits in discrete membrane-trafficking steps. *Molecular biology of the cell*. 2009; 20(12): p. 2885–2899. <https://doi.org/10.1091/mbc.e08-12-1160> PMID: 19386764
16. Horgan C.P., Hanscom S.R., Jolly R.S., Futter C.E., and McCaffrey M.W. Rab11-FIP3 links the Rab11 GTPase and cytoplasmic dynein to mediate transport to the endosomal-recycling compartment. *Journal of cell science*. 2010; 123(Pt 2): p. 181–191. <https://doi.org/10.1242/jcs.052670> PMID: 20026645
17. Jones L.A., Villemant C., Starborg T., Salter A., Goddard G., Ruane P., Woodman P.G., Papalopulu N., et al. Dynein light intermediate chains maintain spindle bipolarity by functioning in centriole cohesion. *The Journal of cell biology*. 2014 207(4): p. 499–516. <https://doi.org/10.1083/jcb.201408025> PMID: 25422374
18. Zhang J., Li S., Musa S., Zhou H., and Xiang X. Dynein light intermediate chain in *Aspergillus nidulans* is essential for the interaction between heavy and intermediate chains. *The Journal of biological chemistry*. 2009. 284(50): p. 34760–34768. <https://doi.org/10.1074/jbc.M109.026872> PMID: 19837669
19. Banks G.T., Haas M.A., Line S., Shepherd H.L., Alqatari M., Stewart S., et al. Behavioral and other phenotypes in a cytoplasmic Dynein light intermediate chain 1 mutant mouse. *The Journal of neuroscience: the official journal of the Society for Neuroscience*. 2011; 31(14): p. 5483–5494.
20. Kong S., Du X., Du X., Peng C., Wu Y., Li H., et al. Dlic1 deficiency impairs ciliogenesis of photoreceptors by destabilizing dynein. *Cell research*. 2013; 23(6): p. 835–850. <https://doi.org/10.1038/cr.2013.59> PMID: 23628724
21. Whyte L.S., Lau A.A., Hemsley K.M., Hopwood J.J., and Sargeant T.J. Endo-lysosomal and autophagic dysfunction: a driving factor in Alzheimer's disease? *Journal of neurochemistry*. 2017; 140(5): p. 703–717. <https://doi.org/10.1111/jnc.13935> PMID: 28027395
22. Vijayan V. and Verstreken P. Autophagy in the presynaptic compartment in health and disease. *The Journal of cell biology*. 2017; 216(7): p. 1895–1906. <https://doi.org/10.1083/jcb.201611113> PMID: 28515275
23. Muller S., Brun S., René F., de Sèze J., Loeffler J.-P., and Jeltsch-David H. Autophagy in neuroinflammatory diseases. *Autoimmunity reviews*. 2017; 16(8): p. 856–874. <https://doi.org/10.1016/j.autrev.2017.05.015> PMID: 28572049

24. Fu X., Sun X., Zhang L., Jin Y., Chai R., Yang L., et al. Tuberosclerosis complex-mediated mTORC1 overactivation promotes age-related hearing loss. *The Journal of clinical investigation*. 2018; 128(11): p. 4938–4955. <https://doi.org/10.1172/JCI98058> PMID: 30247156
25. He Z., Guo L., Shu Y., Fang Q., Zhou H., Liu Y., et al. Autophagy protects auditory hair cells against neomycin-induced damage. *Autophagy*. 2017; 13(11): p. 1884–1904. <https://doi.org/10.1080/15548627.2017.1359449> PMID: 28968134
26. Wu F., Xiong H., and Sha S. Noise-induced loss of sensory hair cells is mediated by ROS/AMPK α pathway. *Redox biology*. 2020; 29: p. 101406–101406. <https://doi.org/10.1016/j.redox.2019.101406> PMID: 31926629
27. Eskelinen E.-L. Maturation of autophagic vacuoles in Mammalian cells. *Autophagy*. 2005; 1(1). <https://doi.org/10.4161/autophagy.1.1.1270> PMID: 16874026
28. Kurtishi A., Rosen B., Patil K.S., Alves G.W., and Møller S.G. Cellular Proteostasis in Neurodegeneration. *Molecular neurobiology*. 2019; 56(5): p. 3676–3689. <https://doi.org/10.1007/s12035-018-1334-z> PMID: 30182337
29. Lumkwana D., du Toit A., Kinnear C., and Loos B. Autophagic flux control in neurodegeneration: Progress and precision targeting—Where do we stand? *Progress in neurobiology*. 2017; 153: p. 64–85. <https://doi.org/10.1016/j.pneurobio.2017.03.006> PMID: 28385648
30. Liu J., Liu W., Lu Y., Tian H., Duan C., Lu L., et al. Piperlongumine restores the balance of autophagy and apoptosis by increasing BCL2 phosphorylation in rotenone-induced Parkinson disease models. *Autophagy*. 2018; 14(5): p. 845–861. <https://doi.org/10.1080/15548627.2017.1390636> PMID: 29433359
31. Ye B., Fan C., Shen Y., Wang Q., Hu H., and Xiang M. The Antioxidative Role of Autophagy in Hearing Loss. *Frontiers in neuroscience*. 2019; 12: p. 1010–1010. <https://doi.org/10.3389/fnins.2018.01010> PMID: 30686976
32. Cason S.E., Carman P.J., Van Duyne C., Goldsmith J., Dominguez R., and Holzbaur E.L.F., Sequential dynein effectors regulate axonal autophagosome motility in a maturation-dependent pathway. *J Cell Biol*. 2021; 220(7).
33. Di Bartolomeo S., Corazzari M., Nazio F., Oliverio S., Lisi G., Antonioni M., et al. The dynamic interaction of AMBRA1 with the dynein motor complex regulates mammalian autophagy. *The Journal of cell biology*. 2010; 191(1): p. 155–168. <https://doi.org/10.1083/jcb.201002100> PMID: 20921139
34. Fimia G.M., Di Bartolomeo S., Piacentini M., and Cecconi F. Unleashing the Ambra1-Beclin 1 complex from dynein chains: Ulk1 sets Ambra1 free to induce autophagy. *Autophagy*. 2011; 7(1): p. 115–117. <https://doi.org/10.4161/autophagy.7.1.14071> PMID: 21079415
35. Ravikumar B., Acevedo-Arozena A., Imarisio S., Berger Z., Vacher C., O’Kane C.J., et al. Dynein mutations impair autophagic clearance of aggregate-prone proteins. *Nature Genetics*. 2005; 37(7): p. 771–776. <https://doi.org/10.1038/ng1591> PMID: 15980862
36. Rubinsztein D.C., Ravikumar B., Acevedo-Arozena A., Imarisio S., O’Kane C.J., and Brown S.D.M. Dyneins, autophagy, aggregation and neurodegeneration. *Autophagy*. 2005; 1(3): p. 177–178. <https://doi.org/10.4161/autophagy.1.3.2050> PMID: 16874055
37. Cristofani R., Crippa V., Rusmini P., Cicardi M.E., Meroni M., Licata N.V., et al. Inhibition of retrograde transport modulates misfolded protein accumulation and clearance in motoneuron diseases. *Autophagy*. 2017; 13(8): p. 1280–1303. <https://doi.org/10.1080/15548627.2017.1308985> PMID: 28402699
38. Tammineni P. and Cai Q. Defective retrograde transport impairs autophagic clearance in Alzheimer disease neurons. *Autophagy*. 2017; 13(5): p. 982–984. <https://doi.org/10.1080/15548627.2017.1291114> PMID: 28318364
39. Tammineni P., Ye X., Feng T., Aikal D., and Cai Q. Impaired retrograde transport of axonal autophagosomes contributes to autophagic stress in Alzheimer’s disease neurons. *Elife*. 2017; 6: e21776. <https://doi.org/10.7554/eLife.21776> PMID: 28085665
40. Chen Y., Li L., Ni W., Zhang Y., Sun S., Miao D., et al. Bmi1 regulates auditory hair cell survival by maintaining redox balance. *Cell Death Dis*. 2015; 6: p. e1605. <https://doi.org/10.1038/cddis.2014.549> PMID: 25611380
41. Pauley S., Lai E., and Fritsch B. Foxg1 is required for morphogenesis and histogenesis of the mammalian inner ear. *Dev Dyn*. 2006; 235(9): p. 2470–82. <https://doi.org/10.1002/dvdy.20839> PMID: 16691564
42. Zhang S., Zhang Y., Dong Y., Guo L., Zhang Z., Shao B., et al. Knockdown of Foxg1 in supporting cells increases the trans-differentiation of supporting cells into hair cells in the neonatal mouse cochlea. *Cellular and molecular life sciences*. 2020. 77(7): p. 1401–1419. <https://doi.org/10.1007/s00018-019-03291-2> PMID: 31485717

43. Li B., Hu Q., Wang H., Man N., Ren H., Wen L., et al. Omi/HtrA2 is a positive regulator of autophagy that facilitates the degradation of mutant proteins involved in neurodegenerative diseases. *Cell death and differentiation*. 2010; 17(11): p. 1773–1784. <https://doi.org/10.1038/cdd.2010.55> PMID: 20467442
44. Ren H., Fu K., Mu C., Li B., Wang D., and Wang G. DJ-1, a cancer and Parkinson's disease associated protein, regulates autophagy through JNK pathway in cancer cells. *Cancer letters*. 2010; 297(1): p. 101–108. <https://doi.org/10.1016/j.canlet.2010.05.001> PMID: 20510502
45. Xia Q., Hu Q., Wang H., Yang H., Gao F., Ren H., et al. Induction of COX-2-PGE2 synthesis by activation of the MAPK/ERK pathway contributes to neuronal death triggered by TDP-43-depleted microglia. *Cell death & disease*. 2015; 6: p. e1702. <https://doi.org/10.1038/cddis.2015.69> PMID: 25811799
46. Yang J., Zhang Y., Hamid S., Cai J., Liu Q., Li H., et al. Interplay between autophagy and apoptosis in selenium deficient cardiomyocytes in chicken. *Journal of inorganic biochemistry*. 2017; 170: p. 17–25. <https://doi.org/10.1016/j.jinorgbio.2017.02.006> PMID: 28214429
47. Khobreakar N.V. and Vallee R.B. A RILP-regulated pathway coordinating autophagosome biogenesis with transport. *Autophagy*. 2020; 16(8): p. 1537–1538. <https://doi.org/10.1080/15548627.2020.1778294> PMID: 32597306
48. Khobreakar N.V., Quintremil S., Dantas T.J., and Vallee R.B. The Dynein Adaptor RILP Controls Neuronal Autophagosome Biogenesis, Transport, and Clearance. *Dev Cell*. 2020; 53(2): p. 141–153.e4. <https://doi.org/10.1016/j.devcel.2020.03.011> PMID: 32275887
49. Kim H.-J., Oh G.-S., Lee J.-H., Lyu A.-R., Ji H.-M., et al. Cisplatin ototoxicity involves cytokines and STAT6 signaling network. *Cell research*. 2011; 21(6): p. 944–956. <https://doi.org/10.1038/cr.2011.27> PMID: 21321603
50. Mizushima N., Yoshimori T., and Levine B. Methods in Mammalian Autophagy Research. *Cell*. 2010; 140(3): p. 313–326. <https://doi.org/10.1016/j.cell.2010.01.028> PMID: 20144757
51. Perlson E., Maday S., Fu M.-M., Moughamian A.J., and Holzbaur E.L.F. Retrograde axonal transport: pathways to cell death? *Trends in neurosciences*. 2010; 33(7): p. 335–344. <https://doi.org/10.1016/j.tins.2010.03.006> PMID: 20434225
52. Ó Maoiléidigh D. and Ricci A.J. A Bundle of Mechanisms: Inner-Ear Hair-Cell Mechanotransduction. *Trends in neurosciences*. 2019; 42(3): p. 221–236. <https://doi.org/10.1016/j.tins.2018.12.006> PMID: 30661717
53. Okamoto S., Chaya T., Omori Y., Kuwahara R., Kubo S., Sakaguchi H., et al. Ick Ciliary Kinase Is Essential for Planar Cell Polarity Formation in Inner Ear Hair Cells and Hearing Function. *The Journal of neuroscience: the official journal of the Society for Neuroscience*. 2017; 37(8): p. 2073–2085. <https://doi.org/10.1523/JNEUROSCI.3067-16.2017> PMID: 28115485
54. Zampini V., Rüttiger L., Johnson S.L., Franz C., Furness D.N., Waldhaus J., Xiong H., et al. Eps8 regulates hair bundle length and functional maturation of mammalian auditory hair cells. *PLoS biology*. 2011; 9(4): p. e1001048. <https://doi.org/10.1371/journal.pbio.1001048> PMID: 21526224
55. Landin Malt A., Dailey Z., Holbrook-Rasmussen J., Zheng Y., Hogan A., Du Q., and Lu X. Par3 is essential for the establishment of planar cell polarity of inner ear hair cells. *Proceedings of the National Academy of Sciences of the United States of America*. 2019; 116(11): p. 4999–5008. <https://doi.org/10.1073/pnas.1816333116> PMID: 30814219
56. Jaarsma D. and Hoogenraad C.C. Cytoplasmic dynein and its regulatory proteins in Golgi pathology in nervous system disorders. *Frontiers in neuroscience*. 2015; 9: p. 397–397. <https://doi.org/10.3389/fnins.2015.00397> PMID: 26578860
57. Yadav S. and Linstedt A.D. Golgi positioning. *Cold Spring Harbor perspectives in biology*. 2011; 3(5). <https://doi.org/10.1101/cshperspect.a005322> PMID: 21504874
58. Lu L. and Hong W. From endosomes to the trans-Golgi network. *Seminars in cell & developmental biology*. 2014; 31: p. 30–39.
59. Corona A.K. and Jackson W.T. Finding the Middle Ground for Autophagic Fusion Requirements. *Trends in cell biology*. 2018; 28(11): p. 869–881. <https://doi.org/10.1016/j.tcb.2018.07.001> PMID: 30115558
60. Xu M., Li X.-X., Xiong J., Xia M., Gulbins E., Zhang Y., et al. Regulation of autophagic flux by dynein-mediated autophagosomes trafficking in mouse coronary arterial myocytes. *Biochimica et biophysica acta*. 2013; 1833(12): p. 3228–3236. <https://doi.org/10.1016/j.bbamcr.2013.09.015> PMID: 24095928
61. Katsumata K., Nishiyama J., Inoue T., Mizushima N., Takeda J., and Yuzaki M. Dynein- and activity-dependent retrograde transport of autophagosomes in neuronal axons. *Autophagy*. 2010; 6(3): p. 378–385. <https://doi.org/10.4161/auto.6.3.11262> PMID: 20150763
62. Schilling G., Becher M.W., Sharp A.H., Jinnah H.A., Duan K., Kotzuc J.A., et al. Intranuclear Inclusions and Neuritic Aggregates in Transgenic Mice Expressing a Mutant N-Terminal Fragment of Huntingtin.

- Human Molecular Genetics. 1999; 8(3): p. 397–407. <https://doi.org/10.1093/hmg/8.3.397> PMID: 9949199
63. Hafezparast M., Klocke R., Ruhrberg C., Marquardt A., Ahmad-Annuar A., Bowen S., Lalli G., et al. Mutations in dynein link motor neuron degeneration to defects in retrograde transport. *Science*. 2003; 300(5620): p. 808–812. <https://doi.org/10.1126/science.1083129> PMID: 12730604
 64. Menzies F.M., Fleming A., Caricasole A., Bento C.F., Andrews S.P., Ashkenazi A., et al. Autophagy and Neurodegeneration: Pathogenic Mechanisms and Therapeutic Opportunities. *Neuron*. 2017; 93(5): p. 1015–1034. <https://doi.org/10.1016/j.neuron.2017.01.022> PMID: 28279350
 65. Clark S.G., Graybeal L.L., Bhattacharjee S., Thomas C., Bhattacharya S., and Cox D.N. Basal autophagy is required for promoting dendritic terminal branching in *Drosophila* sensory neurons. *PloS one*. 2018; 13(11): p. e0206743–e0206743. <https://doi.org/10.1371/journal.pone.0206743> PMID: 30395636
 66. Fujimoto C., Iwasaki S., Urata S., Morishita H., Sakamaki Y., Fujioka M., et al. Autophagy is essential for hearing in mice. *Cell death & disease*. 2017; 8(5): p. e2780. <https://doi.org/10.1038/cddis.2017.194> PMID: 28492547
 67. Magariños M., Pulido S., Aburto M.R., de Iriarte Rodríguez R., and Varela-Nieto I. Autophagy in the Vertebrate Inner Ear. *Frontiers in cell and developmental biology*. 2017; 5: p. 56. <https://doi.org/10.3389/fcell.2017.00056> PMID: 28603711
 68. Mariño G., Fernández A.F., Cabrera S., Lundberg Y.W., Cabanillas R., Rodríguez F., et al. Autophagy is essential for mouse sense of balance. *The Journal of clinical investigation*. 2010; 120(7): p. 2331–2344. <https://doi.org/10.1172/JCI42601> PMID: 20577052
 69. Hyttinen J.M.T., Niittykoski M., Salminen A., and Kaarniranta K. Maturation of autophagosomes and endosomes: a key role for Rab7. *Biochimica et biophysica acta*. 2013; 1833(3): p. 503–510. <https://doi.org/10.1016/j.bbamcr.2012.11.018> PMID: 23220125
 70. Wen H., Zhan L., Chen S., Long L., and Xu E. Rab7 may be a novel therapeutic target for neurologic diseases as a key regulator in autophagy. *Journal of neuroscience research*. 2017; 95(10): p. 1993–2004. <https://doi.org/10.1002/jnr.24034> PMID: 28186670
 71. Vanlandingham P.A. and Ceresa B.P. Rab7 regulates late endocytic trafficking downstream of multivesicular body biogenesis and cargo sequestration. *The Journal of biological chemistry*. 2009; 284(18): p. 12110–12124. <https://doi.org/10.1074/jbc.M809277200> PMID: 19265192
 72. Wong Y.C., Kim S., Peng W., and Krainc D. Regulation and Function of Mitochondria-Lysosome Membrane Contact Sites in Cellular Homeostasis. *Trends in cell biology*. 2019; 29(6): p. 500–513. <https://doi.org/10.1016/j.tcb.2019.02.004> PMID: 30898429
 73. Tan E.H.N. and Tang B.L. Rab7a and Mitophagosome Formation. *Cells*. 2019; 8(3): p. 224. <https://doi.org/10.3390/cells8030224> PMID: 30857122